

Spectral assignments and structural studies of a warfarin derivative stereoselectively formed by tandem cyclization



M. Velayutham Pillai, K. Rajeswari, T. Vidhyasagar*

Department of Chemistry, Annamalai University, Annamalai Nagar, 608 002 Tamil Nadu, India

ARTICLE INFO

Article history:

Received 23 February 2015

Received in revised form

12 July 2015

Accepted 27 July 2015

Available online 30 July 2015

Keywords:

Tandem cyclization

Warfarin derivative

1D and 2D NMR

Single crystal X-ray diffraction

Theoretical studies

ABSTRACT

The structural elucidation of a Mannich condensation product of *rac*-Warfarin with benzaldehyde and methyl amine was carried out using IR, Mass, ^1H NMR, ^{13}C NMR, ^1H – ^1H COSY, ^1H – ^{13}C COSY, DEPT–135, HMBC, NOESY spectra and single crystal X-ray diffraction. Formation of a new pyran ring via a tandem cyclization in the presence of methyl amine was observed. The optimized geometry and HOMO–LUMO energy gap along with other important physical parameters were found by Gaussian 09 program using HF 6–31G (d, p) and B3YLP/DFT 6–31G (d, p) level of theory. The preferred conformation of the piperidine ring in solution state was found to be chair from the NMR spectra. Single crystal X-ray diffraction and optimized geometry (by theoretical study) also confirms the chair conformation in the solid state.

© 2015 Elsevier B.V. All rights reserved.

1. Introduction

2,6-Disubstituted-4-piperidines [1] are being constituents of a number of alkaloids which have broad spectrum of biological activities. Bicyclic systems with *N*-methyl piperidine and pyran units [2] together showed a distinct potential pattern of selectivity towards antitumor activity. Aza spiro systems [3] containing substituted piperidinyl rings exhibit antibacterial and antifungal activities. Antimycobacterial evaluation carried out to explore the biological efficacy of pyran derivatives [4,5] of *N*-methyl piperidone is also known. 4-Hydroxycoumarin derivatives such as Warfarin, Acenocoumarol [6–9] possess anticoagulant and rodenticidal properties. Warfarin is being studied extensively due to its pharmacological properties. Racemic sodium warfarin is the most widely used antithrombotic drug in USA and Canada.

Multicomponent reactions involving three or more different substrates reacting in a well-defined manner to form a single compound has emerged as a powerful tool for synthesizing biologically potent molecules [10]. Tandem reactions often afford stereoselectivity [11–17] of medicinally important structural moieties in a facile manner. It is noteworthy that hybrid molecules play an important role in biological activity. Prompted by these reports,

we have tried to synthesize a molecular hybrid (5) containing both coumarin and substituted piperidine moiety through a one-step Mannich reaction. The reaction proceeded one step further to form a cyclized product (4) containing an additional pyran ring with the expected piperidine and coumarin rings. The structure and stereochemistry of the newly synthesized product is established through IR, Mass, ^1H NMR, ^{13}C NMR, ^1H – ^1H COSY, ^1H – ^{13}C COSY, DEPT–135, HMBC, NOESY spectra and through single crystal X-ray diffraction analysis. Theoretical studies have also been carried out using HF/6–31G (d, p) and B3YLP/DFT 6–31G (d, p) methods to deduce optimized geometry, HOMO–LUMO energy gap, NLO properties and Mulliken charge distribution etc.

2. Experimental

2.1. Synthesis of compound 4

The parent compound *rac*-warfarin (3) was prepared from 4-hydroxycoumarin (1) and benzylidene acetone (2) by the Michael addition reaction as reported in the literature [6]. The title compound 4 was prepared from *rac*-warfarin as follows: A mixture of 1 mmol (0.31 g) of *rac*-warfarin, 2 equivalents (0.21 mL) of benzaldehyde and 2 equivalents (0.17 mL) of methyl amine solution (40% in water) in ethanol was heated to boiling on a hot plate. Colourless crystals thus precipitated on cooling were recrystallized from ethanol to get the product in pure form. Single crystal suitable

* Corresponding author.

E-mail address: tvscchemau@gmail.com (T. Vidhyasagar).

for X-ray diffraction analysis was obtained by slow evaporation of a solution of compound **4** in ethanol.

2.2. Spectral measurements and X-ray diffraction

FT–IR spectrum was recorded on a NICOLET AVATAR 360 FT–IR spectrometer and the pellet technique (KBr) was adopted to record the spectrum. LC–Mass spectrum was recorded on a Shimadzu–LCMS 2010A mass spectrometer.

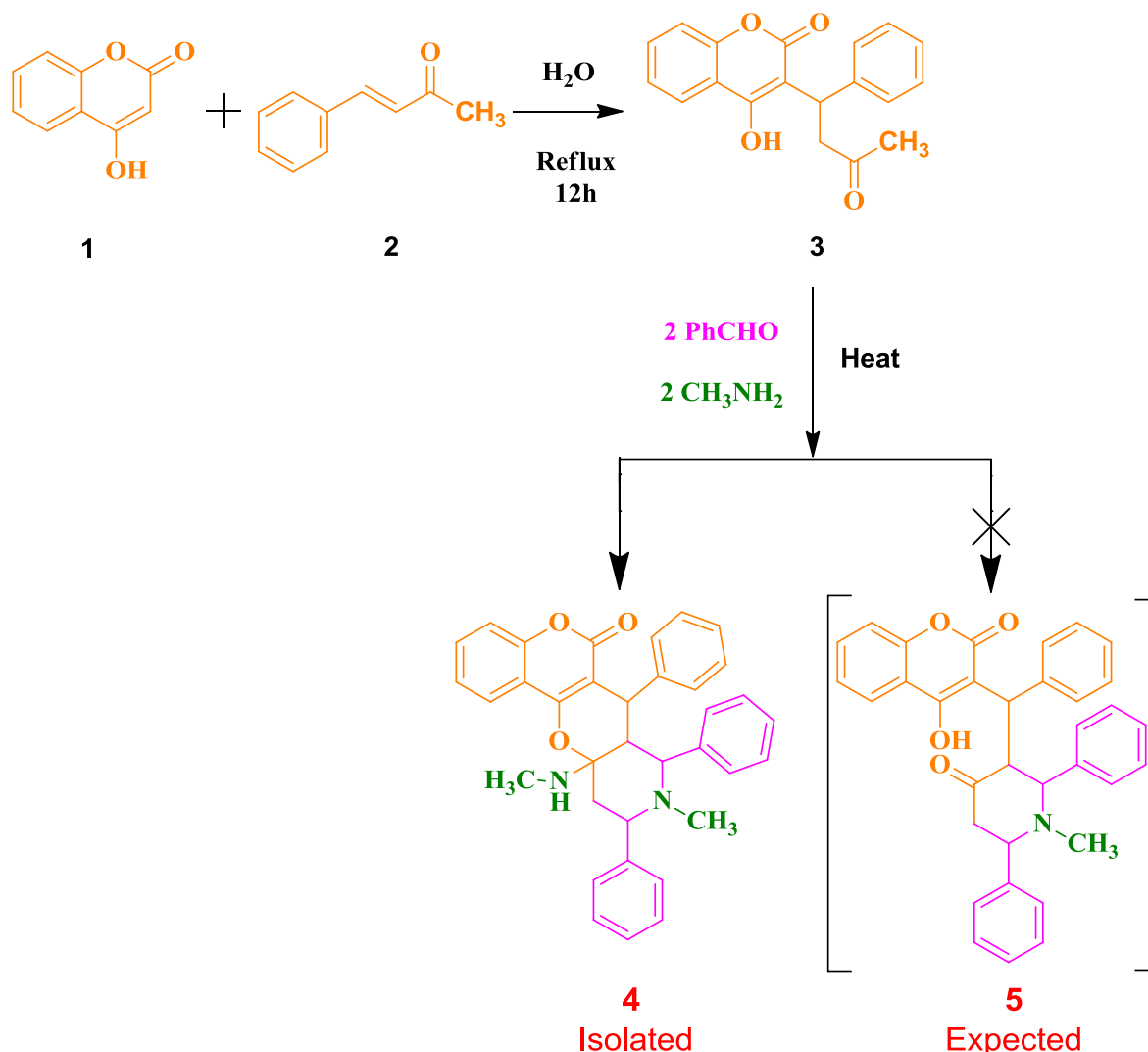
NMR spectra were recorded on a Bruker ULTRASHILED 400 PLUS spectrometer (Bruker Biospin GmbH, Rheinstetten, Germany) at around 294 K. Deuterated chloroform was used as a solvent to dissolve the compound **4**. The quantity of sample (compound **4**) taken for ^1H NMR and ^1H decoupled ^{13}C NMR were 10 mg and 50 mg respectively in 0.5 mL of CDCl_3 . Chemical shifts (δ) are quoted in parts per million (ppm) and are referenced to the TMS, $\delta = 0$ ppm. Spin multiplicities are expressed as singlet (s), doublet (d), triplet (t), doublet of doublets (dd) and multiplet (m). Coupling constants (J) are given in Hz. The ^1H NMR data were acquired at 400 MHz frequency with number of scans = 16, acquisition time = 3.98 s, relaxation time = 1 s, 90° pulse width (P1) = 13.50 μs , spectral width = 8223.685 Hz, line broadening = 0.30 Hz, and FT size = 65,536. A frequency at 100 MHz was observable for ^{13}C NMR

spectrum with number of scans = 2000, acquisition time = 1.36 s, relaxation time = 2 s, 90° pulse width (P1) = 8.25 μs , spectral width = 24,038.461 Hz, line broadening = 1.00 Hz, and FT size = 32,768. ^1H – ^1H COSY, ^1H – ^{13}C COSY, HMBC, DEPT–135 and NOESY spectra were measured with the pulse sequence gcosy, ghsqc, ghmbc, deptsp 135 and noesy respectively.

Single crystal X-ray diffraction analysis was carried out at 298 K using a three circle Bruker SMART–APEX CCD area detector system under Mo $K\alpha$ ($\lambda = 0.71073 \text{ \AA}$) graphite monochromated X-ray beam with a crystal to detector distance of 60 mm and a collimator of 0.5 mm. The total number of reflections was equal to 5582. The structural refinement was done using SHELXL 97 by full–matrix least–squares method with anisotropic temperature parameter for all non-hydrogen atoms.

2.3. Theoretical calculations

Theoretical calculations were done by considering the crystal structure of compound **4** as the initial structure using HF and B3LYP/DFT methods using 6–31G (d, p) as the basis set in Gaussian 09 package [18] to optimize the structure. The lowest unoccupied molecular orbital (LUMO) and highest occupied molecular orbital (HOMO) energy differences for the molecule were calculated by



Scheme 1. Synthetic scheme of compound **4**.

Table 1
 ^1H (400 MHz) and ^{13}C NMR (100 MHz) spectroscopic data of compound **4** (in CDCl_3).

Atom number	δ_{H} (ppm)	δ_{C} (ppm)
1	8.07 (d, 1H, $J = 7.6$ Hz, H1)	122.8 (C1)
2	7.36 (t, 3H, Ar–H)(H2 and H4 – merged with phenyl ring proton signal)	124.0 (C2)
3	7.64 (t, 1H, $J = 8$ Hz, H3)	132.0 (C3)
4	7.36 (t, 3H, Ar–H) (H2 and H4 – merged with phenyl ring proton signal)	116.9 (C4)
4a	–	153.2 (C4a)
6	–	162.3 (C6)
6a	–	92.9 (C6a)
7	3.97 (s, 1H, H7)	36.1 (C7)
7a	2.89 (d, 1H, $J = 10.8$ Hz, H7a)	50.3 (C7a)
8	2.95 (d, 1H, $J = 10.8$ Hz, H8)	71.3 (C8)
9	1.68 (s, 3H, N9– CH_3)	42.0 (NCH ₃)
10	3.35 (d, 1H, $J = 9.6$ Hz, H10)	65.5 (C10)
11	2.05 (t, 1H, $J = 13.6$ Hz, H11ax) 2.63 (dd, 1H, $J = 14.4$ Hz, 2.4 Hz, H11eq)	43.0 (C11)
11a	2.17 (s, 3H, NH– CH_3) 3.48 (s, 1H, NH– CH_3)	26.4 (NHCH ₃) 99.6 (C11a)
12a	–	159.3 (C12a)
13	–	115.9 (C13)
Phenyl rings	6.85 (d, 2H, $J = 7.6$ Hz, Ar–H) 7.11 (t, 1H, $J = 7.6$ Hz, Ar–H) 7.19 (t, 2H, $J = 7.6$ Hz, Ar–H) 7.30 (t, 2H, $J = 7.2$ Hz, Ar–H) 7.36 (t, 3H, Ar–H)(H2 and H4 – merged with phenyl ring proton signal) 7.43 (t, 3H, $J = 8.4$ Hz, Ar–H) 7.89 (bs, 1H, Ar–H)	142.2, 142.5, 144.0 (<i>ipso</i> carbons) 126.3, 126.7, 127.1, 127.4, 128.1, 128.7, 128.9, 129.1, 129.6, 131.1 (Others)

these methods. The other properties like bond lengths, bond angles, dihedral angles, dipole moment, polarizability, hyperpolarizability and Mulliken charge distribution pattern and some other important molecular properties are also calculated using the same package. Gauss View program is used to visualize the results obtained from calculations, which were made by Gaussian 09 program.

3. Results and discussion

3.1. General

The reaction between 1 mmol of *rac*-warfarin (**3**), 2 eq. benzaldehyde and 2 eq. methyl amine (40% in water) in ethanol at boiling condition has resulted the precipitation of the crystalline

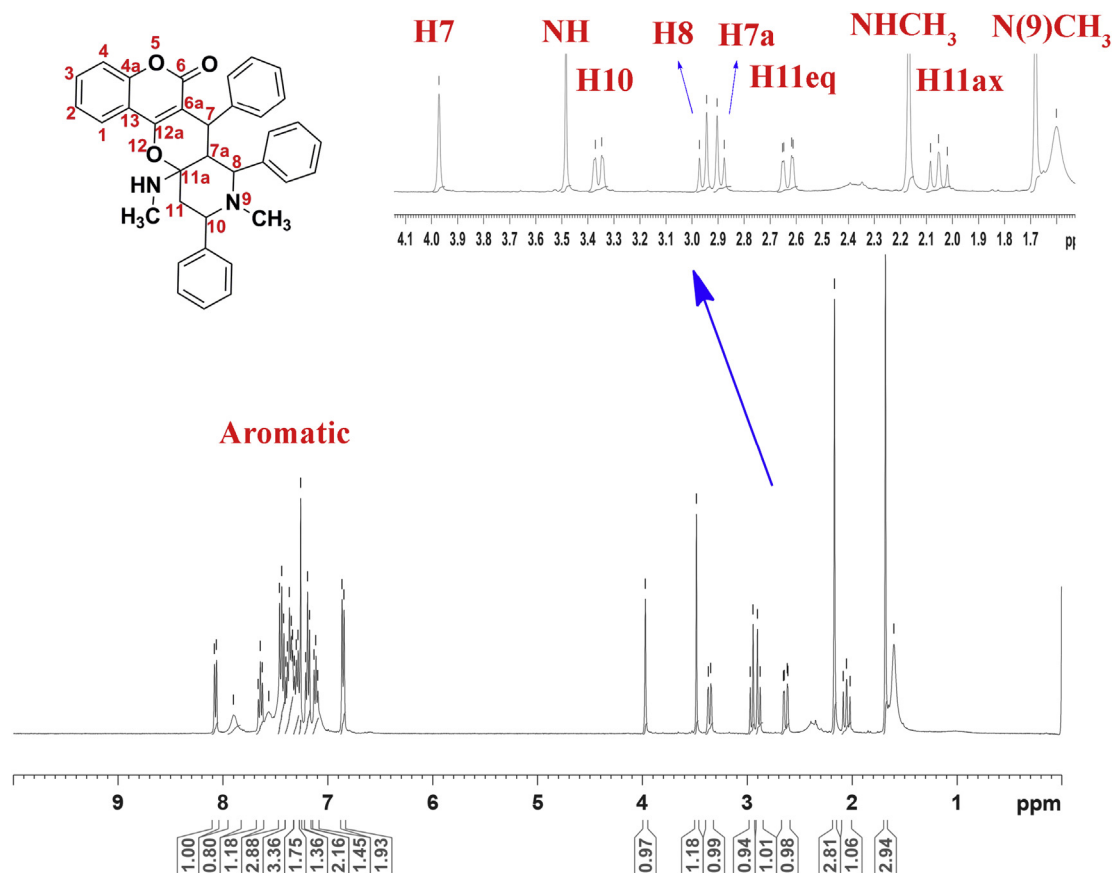


Fig. 1. ^1H NMR spectrum of compound **4**.

product: 9-methyl-11a-(methylamino)-7,8,10-triphenyl-7a,8,9,10,11,11a-hexahydrochromeno [3',4':5,6]pyrano[3,2-c]pyridin-6(7H)-one (**4**). The synthetic scheme of compound **4** is shown in Scheme 1. Recrystallization of the crude product from ethanol gave the pure product (yield 68%).

The Michael addition of 4-hydroxycoumarin (**1**) with benzylidene acetone (**2**) in water heated to reflux condition gives 4-hydroxy-3-(3-oxo-1-phenylbutyl)-2H-chromen-2-one which is also known as *rac*-warfarin (**3**). Warfarin undergoes Mannich condensation with 2 equivalents of benzaldehyde and 1 equivalent of methylamine forms 3-[(4-hydroxy-2-oxo-2H-chromen-3-yl) (phenyl)methyl]-1-methyl-2,6-diphenylpiperidin-4-one (**5**) which on enamination at the ketonic carbonyl group of piperidine ring by means of methylamine followed by cyclization with the enolic group of the coumarin moiety to give the title compound **4** stereoselectively in such a way that the cyclization resulted in the formation of a pyran ring and a new stereogenic centre.

3.2. Spectral assignments

3.2.1. FT-IR and LC-MASS spectra

FT-IR spectrum of compound **4** (Fig. S6 in the supplementary file) showed peaks at 3389 (N-H stretching), 1705 (C=O stretching), 1619 (C=C stretching), 1199 (C-O stretching) and others which confirmed the product formation. Further, LC-Mass spectrum (Fig. S7 given in the supplementary data) also displayed base peak at $m/z = 529$ representing $(M + H)^+$ ion thereby substantiated the product formation.

3.2.2. ^1H NMR spectrum

The ^1H and ^{13}C chemical shift values are furnished in Table 1. The signals in the ^1H (Fig. 1) and ^{13}C NMR spectra (Fig. 2) of compound **4** were assigned based on their chemical shift, splitting pattern, coupling constant values, correlations in the 2D NMR spectra and comparison with the ^1H and ^{13}C NMR spectral data of 4-hydroxycoumarin available from spectral database for organic compounds (SDBS) [19]. Selected ^1H - ^1H COSY, ^1H - ^{13}C COSY, HMBC and NOE correlations of compound **4** (Table 2) are illustrated through Fig. 3. The methyl protons of NCH_3 and NHCH_3 group are resonating at 1.68 ppm and 2.16 ppm respectively as readily recognizable signals in the ^1H NMR spectrum. In the ^1H - ^1H COSY spectrum (Fig. S1 in supplementary files), three signals respectively at 3.35 ppm, 2.63 ppm and 2.05 ppm correlated among themselves represent H10, H11eq and H11ax protons forming an AMX spin system of coupling. This assignment is confirmed by their coupling constant values observed [$^3J_{(\text{H}10\text{ax}, \text{H}11\text{ax})} = 9.6$ Hz, $^2J_{(\text{H}11\text{eq}, \text{H}11\text{ax})} = 14.4$ Hz, and $^3J_{(\text{H}11\text{eq}, \text{H}10\text{ax})} = 2.4$ Hz]. A one proton singlet at 3.97 ppm correlated to one of the protons of the AB spin system at 2.89 ppm with a coupling constant of 10.8 Hz represents H7 and H7a protons which are characteristic of vicinal protons orienting *trans* axially to each other. Further, the correlation between one of the proton signal of AB spin system at 2.95 ppm ($J = 10.8$ Hz) with the carbon signal at 71.3 ppm in the ^1H - ^{13}C COSY spectrum (Fig. S2 in supplementary file) indicates the former as H8. The one proton signal at 3.48 ppm assigned to amino proton (NH) is substantiated by D_2O exchange process (Spectrum shown in the supplementary file).

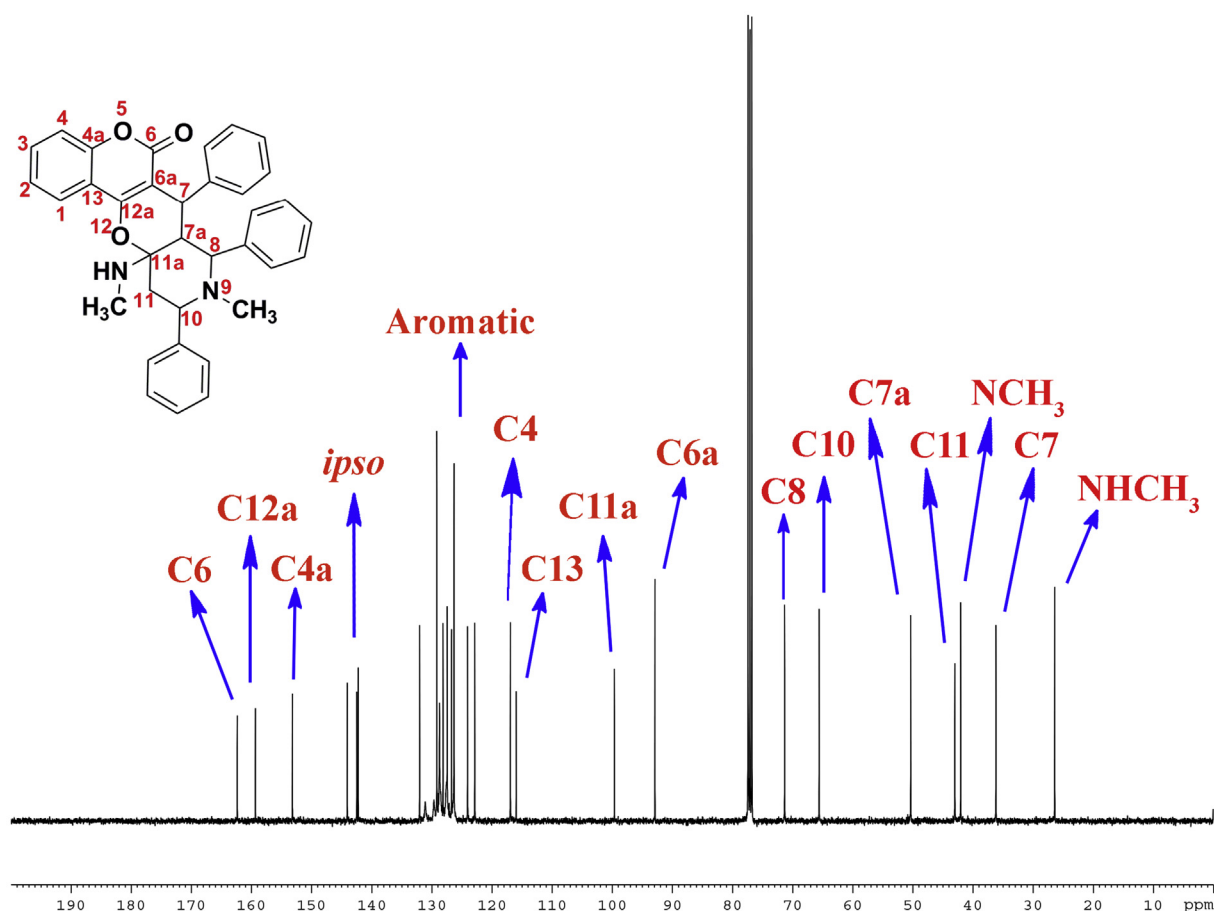


Fig. 2. ^{13}C NMR spectrum of compound **4**.

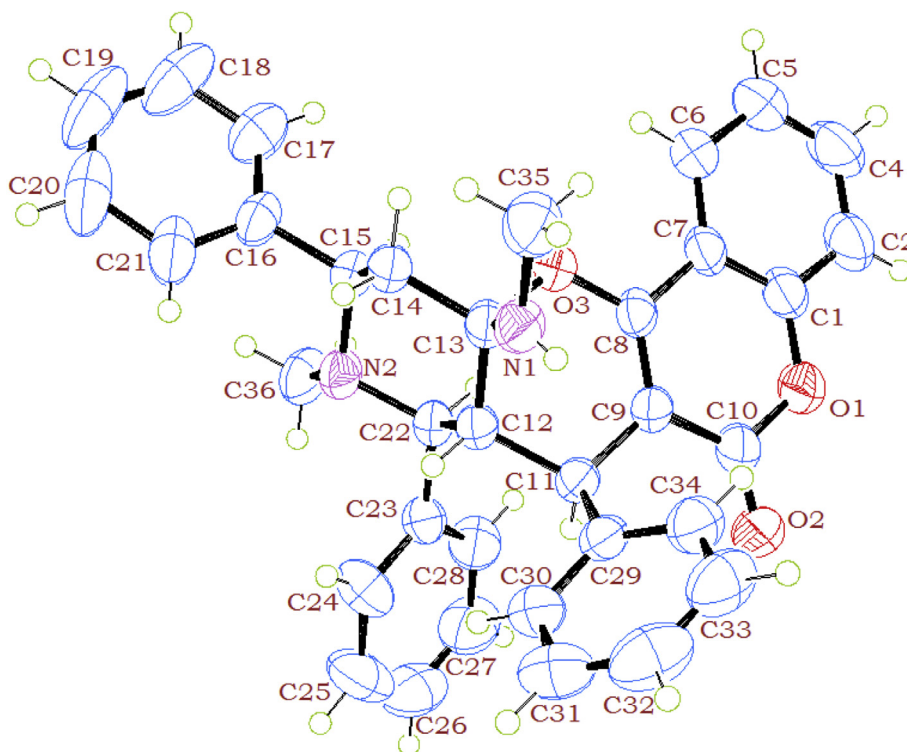


Fig. 4. ORTEP of compound 4 drawn at 50% probability level.

conformational preference of the pyran ring present in the molecule is deducible as half-chair from X-ray crystallography.

3.2.5. Single crystal X-ray diffraction analysis

The single crystal X-ray diffraction analysis [20] of compound 4 was carried out to find the solid state geometry. A summary of data obtained from the analysis is illustrated through Table S1 (in the supplementary file). The ORTEP drawn at 50% probability level is

shown in Fig. 4. The crystal belongs to triclinic system with the space group $P\bar{1}$. In this molecule, piperidine ring adopts a chair conformation with equatorial orientation of substituents while the pyran ring exists in a half chair conformation. The torsion angle $O3-C13-C12-C11 = 60.0^\circ$ suggests that in the piperidine ring, $C13-O3$ bond is axially oriented which resulted in the equatorial orientation of the $C13-N1$ bond (torsion angle $N1-C13-C12-C22 = 173.5^\circ$).

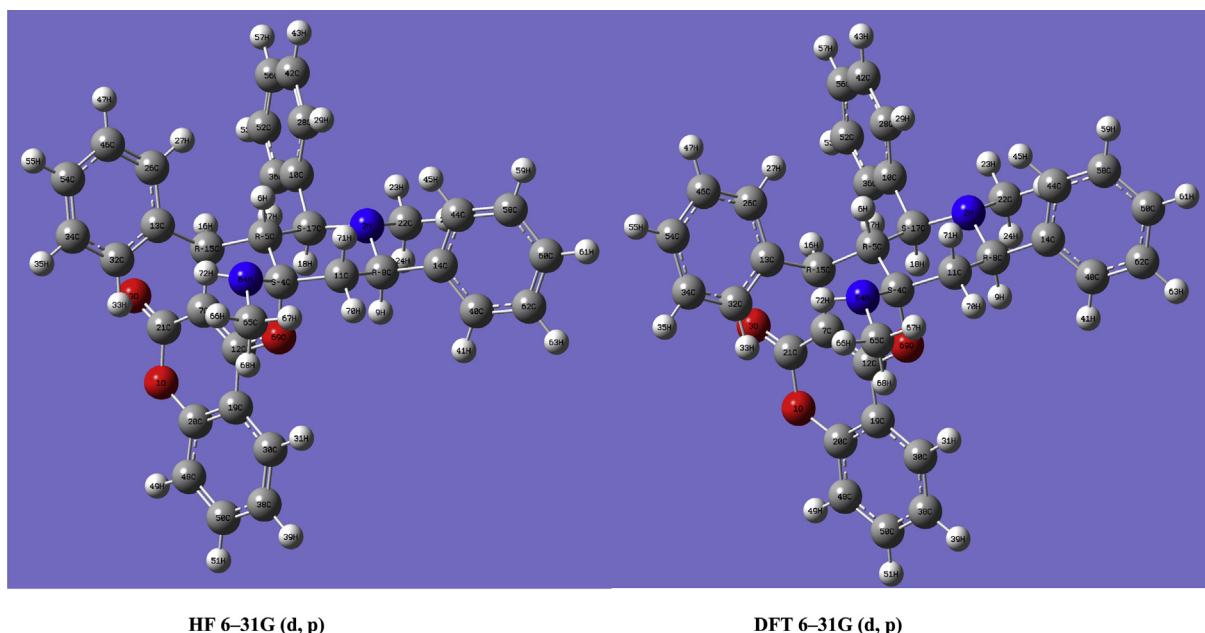


Fig. 5. Optimized structure of compound 4 by HF 6–31G (d, p) and DFT 6–31G (d, p).

3.3. Theoretical study

3.3.1. Molecular geometry

Theoretical study has been carried out using HF/6–31G (d, p) and B3LYP/DFT 6–31G (d, p) methods in Gaussian 09 program. The full geometry optimization was carried out using 6–31G (d, p) basis set both by HF and DFT methods. The optimized geometry for the molecule predicted in the gas phase is shown in Fig. 5 and the optimization parameters such as bond lengths, bond angles and dihedral angles along with the experimental data obtained from X-ray diffraction are given in the Table S2 (in supplementary file) for comparative purpose. From the table, it is noticeable that there is considerable agreement between theoretical and experimental values of parameters such as bond lengths, bond angles. Despite some deviations in bond angles and dihedral angles, the stereochemical orientations of the substituents are not changed much. The variations observed between theoretical and experimental parameters could be understandable from the fact that in the solid state, intra as well as intermolecular interactions (such as hydrogen bonding and van der Waal's forces of attraction) play an important role in the molecular packing and stability of the molecule. Moreover, in the theoretical study an isolated molecule in the gaseous state is considered for calculations.

3.3.2. HOMO–LUMO energies

The HOMO and LUMO energies calculated by HF 6–31G (d, p) are -8.7890 eV and -5.4422 eV respectively while that by DFT 6–31G (d, p) are -8.7639 eV and -5.4776 eV respectively. The LUMO and HOMO are being measures of electron affinity (A) and ionization energy (I) as $-E_{\text{LUMO}} = A$ and $-E_{\text{HOMO}} = I$ respectively. The energy gap between the LUMO and HOMO is also indicative of the global hardness ($\eta = \frac{1}{2}[E_{\text{LUMO}} - E_{\text{HOMO}}]$) which is associated with the stability of the system while the term chemical potential (μ) is given by $\frac{1}{2}[E_{\text{LUMO}} + E_{\text{HOMO}}]$. Further, the global electrophilicity index (ω) is derived from the relation $\omega = \mu^2/2\eta$. The above molecular properties calculated are depicted in Table S3 (in the supplementary file). The energy gap between the HOMO and the LUMO as calculated by HF and DFT methods are 3.3468 eV and 3.2863 eV respectively which suggests that the molecule is soft, more polarizable, associated with appreciable chemical reactivity. Moreover, the HOMO and LUMO energy gap explains the eventual charge transfer interactions that take place within the molecule which are responsible for the bioactivity of the molecule.

The HOMO and LUMO diagrams of compound **4** as predicted by HF and DFT methods are shown in Fig. 6. It is observed from the HOMO and LUMO orbital diagrams [HF 6–31G (d, p)] that in the HOMO, the electron density is localized mainly over the piperidine ring only while in the LUMO; the electron density is distributed mainly over the coumarin ring only and this also indicates that the HOMO is made up of σ -type and LUMO is mostly π -type orbitals. The HOMO–LUMO diagram as per the DFT method reveals that the electron density in HOMO is concentrated mainly in the piperidine ring and there is only a partial distribution of electrons over phenyl and coumarin rings. However, the LUMO has the electron density in the coumarin and piperidine part but the phenyl rings attached to the piperidine ring don't contribute to the LUMO and the phenyl ring attached to the pyran ring is having a partial electron delocalization over it. It is notable that, when electronic transitions occur from HOMO to LUMO in the molecule, electron density significantly increases in the coumarin ring which thereby behaves as an electron acceptor in the molecule and the remaining part of the molecule act as the electron donor.

3.3.3. NLO properties

The NLO properties such as dipole moment, polarizability and

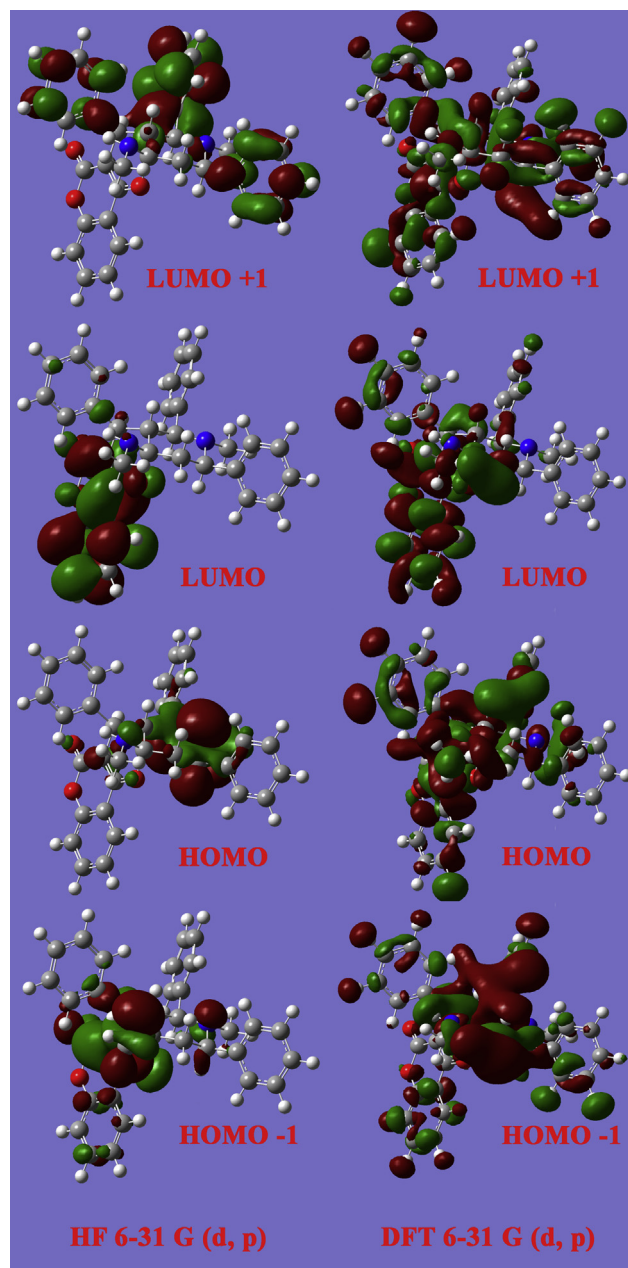


Fig. 6. HOMO and LUMO diagrams of compound **4**.

hyperpolarizability calculated by theoretical study are shown in Table S4 (in supplementary file). The dipole moment value equal to 4.2929 D (HF) and/or 3.9144 D (DFT) indicates the polar nature of the molecule. The highest value of dipole moment is observed for the component μ_y equal to 2.7613 (HF) and/or 1.9532 (DFT) in the molecule. The calculated polarizability is higher for the component $\alpha_{yy} = -203.757$ (HF) and/or -205.343 (DFT) and the hyperpolarizability is higher for the β_{xxx} component [75.9377 (HF) and/or 66.0241 (DFT)]. It is interesting to note that the calculated polarizability (α) value for compound **4** is equal to 62.209×10^{-24} e.s.u. (HF) and/or 61.119×10^{-24} e.s.u. (DFT) which is almost $2\frac{1}{2}$ times greater than that of *p*-nitroaniline, a typical NLO material [21,22]. Also the comparison of hyperpolarizability [β , 0.98719×10^{-30} e.s.u. (HF) and/or 0.82098×10^{-30} e.s.u. (DFT)] of compound **4** (which is greater than that of the standard NLO material urea [23], $\beta = 0.72137 \times 10^{-30}$ e.s.u.) reveals that the former could be used as

an effective NLO material.

3.3.4. Atomic charge distribution

The charge distribution on a molecule has a significant influence on dipole moment, molecular polarizability, electronic structure, vibrational spectra and other properties of molecular systems. Mulliken atomic charge distribution is calculated for compound **4** and the table summarizing the charge distribution is given along with the graph explaining the same pictorially in the [supplementary file \(Table S5 and Fig. S8\)](#). It is seen from the graph that the heteroatoms O1, N2, O3, N64 and O69 (atom numbering is as per the theoretical study) are accumulated with negative charges as a result of molecular relaxation and these atoms behave as electron acceptors. There is a large accumulation of positive charge on C21 and a large negative charge on O69 atoms. It is also notable that both oxygen and nitrogen atoms are having equal negative charges. The excess is taken from the nearby carbon and hydrogen atoms and as a result of this they are found with positive sign in the graph. Further, most of the carbon atoms are negatively charged indicating the charge transfers that occur from hydrogen atoms to carbon atoms in the molecule.

4. Conclusion

A novel heteroaromatic product formed stereoselectively by tandem sequence of reactions between *rac*-wararin, benzaldehyde and methylamine was characterized through IR, Mass, ^1H and ^{13}C NMR, ^1H – ^1H COSY, ^1H – ^{13}C COSY, DEPT-135, HMBC, NOESY spectra and single crystal X-Ray diffraction. The conformation in the solution state of the piperidine ring is found to be chair and that of pyran ring is half chair as per the NMR and single crystal data. The optimized geometry of the molecule was found from theoretical calculation using HF 6-31G (d, p) and B3YLP/DFT 6-31G (d, p) level of theory in Gaussian 09 program and compared with the experimental results.

Appendix A. Supplementary data

Supplementary data related to this article can be found at <http://dx.doi.org/10.1016/j.molstruc.2015.07.058>.

References

[1] a) M. Rubiralta, E. Giralt, A. Diez, in: *Piperidine Structure, Preparation and*

- Synthetic Applications of Piperidine and its Derivatives*, Elsevier, Amsterdam, 1991;
- b) M.W. Edwards, H.M. Garraffo, J.W. Daly, *Synthesis* 11 (1994) 1167–1170.
- [2] H.I. El-Subbagh, S.M. Abu-Zaid, M.A. Mahran, F.A. Badria, A.M. Al-Obaid, *J. Med. Chem.* 43 (2000) 2915–2921.
- [3] S. Balasubramanian, C. Ramalingam, G. Aridoss, S. Kabilan, *Eur. J. Med. Chem.* 40 (2005) 694–700.
- [4] R. Ranjith Kumar, S. Perumal, P. Senthilkumar, P. Yogeewari, D. Sriram, *Bio-org. Med. Chem. Lett.* 17 (2007) 6459–6462.
- [5] R. Ranjith Kumar, S. Perumal, J. Carlos Menendez, P. Yogeewari, D. Sriram, *Bioorg. Med. Chem. Lett.* 19 (2011) 3444–3450.
- [6] M. Ikawa, M.A. Stahman, K.P. Link, *J. Am. Chem. Soc.* 66 (1944) 902–906.
- [7] M. Ikawa, M. Stahman, K. Link, U.S. Patent. (1947) 2,427,578; *Chem. Abstr.* 42, p603h.
- [8] W. Stoll, F. Litwan, U.S. Patent (1953) 2,648,682.
- [9] J.R. Geigy, A.G. Basel, *Chem. Abstr.* 49 (1955) p2522fg.
- [10] The Merck Index, M. Windholz, Ed. 10th Ed, Rahway, USA, 5.
- [11] S. Malaquin, M. Jida, J. Gesquiere, R. Deprez–Poulain, B. Deprez, G. Laconde, *Tetrahedron Lett.* 51 (2010) 2983–2985.
- [12] N. Savitha Devi, S. Perumal, *Tetrahedron* 62 (2006) 5931–5936.
- [13] M. Srinivasan, S. Perumal, *Tetrahedron* 62 (2006) 7726–7732.
- [14] M.N. Elinson, A.N. Vereshchagin, S.K. Feducovich, T.A. Zaimovskaya, Z.A. Starikova, P.A. Belyakov, G.I. Nikishin, *Tetrahedron Lett.* 48 (2007) 6614–6619.
- [15] S. Indumathi, R. Ranjith Kumar, S. Perumal, *Tetrahedron* 63 (2007) 1411–1416.
- [16] N. Ayyagari, D. Jose, S.M. Mobin, I.N.N. Namboothiri, *Tetrahedron Lett.* 52 (2011) 258–262.
- [17] P.S. Harikrishnan, S.M. Rajesh, S. Perumal, *Tetrahedron Lett.* 53 (2012) 3880–3884.
- [18] M. J. Frisch, G. W. Trucks, H. B. Schlegel, G. E. Scuseria, M. A. Robb, J. R. Cheeseman, G. Scalmani, V. Barone, B. Mennucci, G. A. Petersson, H. Nakatsuji, M. Caricato, X. Li, H. P. Hratchian, A. F. Izmaylov, J. Bloino, G. Zheng, J. L. Sonnenberg, M. Hada, M. Ehara, K. Toyota, R. Fukuda, J. Hasegawa, M. Ishida, T. Nakajima, Y. Honda, O. Kitao, H. Nakai, T. Vreven, J. A. Montgomery, Jr., J. E. Peralta, F. Ogliaro, M. Bearpark, J. J. Heyd, E. Brothers, K. N. Kudin, V. N. Staroverov, R. Kobayashi, J. Normand, K. Raghavachari, A. Rendell, J. C. Burant, S. S. Iyengar, J. Tomasi, M. Cossi, N. Rega, J. M. Millam, M. Klene, J. E. Knox, J. B. Cross, V. Bakken, C. Adamo, J. Jaramillo, R. Gomperts, R. E. Stratmann, O. Yazyev, A. J. Austin, R. Cammi, C. Pomelli, J. W. Ochterski, R. L. Martin, K. Morokuma, V. G. Zakrzewski, G. A. Voth, P. Salvador, J. J. Dannenberg, S. Dapprich, A. D. Daniels, O. Farkas, J. B. Foresman, J. V. Ortiz, J. Cioslowski, and D. J. Fox, Gaussian Inc., Wallingford CT, 2009.
- [19] Structure Data Base (SDBS) Website: <http://www.sdb.sdb.aist.go.jp>.
- [20] Crystallographic data of compound **4** have been deposited with the Cambridge Crystallographic Data Centre as publication number CCDC 995847. Copy of the data can be obtained free of charge from CCDC, 12 Union Road, Cambridge CB2 1EZ, UK [Fax: +44(0) 1223 336033 or through e-mail: deposit@ccdc.cam.ac.uk].
- [21] L. T. Cheng, W. Tam, S. H. Stevenson, G. R. Meredith, G. Rikken, S. R. Marder, *J. Phys. Chem.* 95(1191) 10631–10643.
- [22] P. Kaatz, E.A. Donley, D.P. Shelton, *J. Chem. Phys.* 108 (1998) 849–856.
- [23] a) J. Gerratt, I.M. Mills, *J. Chem. Phys.* 49 (1968) 1719–1729;
- b) P. Pulay, *J. Chem. Phys.* 78 (1983) 5043–5051;
- c) Y. Osamura, Y. Yamaguchi, H.F. Schaefer III, *J. Chem. Phys.* 77 (1982) 383–390;
- d) C.E. Dykstra, P.G. Jasien, *Chem. Phys. Lett.* 109 (1984) 388–393.